Fabrication and Catalytic Performance of Au/3DOM Fe_2O_3 Catalysts for the Oxidative Removal of Toluene

Jun Yang, Xingtian Zhao, Shaohua Xie, Jiguang Deng, Hongxing Dai*
Department of Chemistry and Chemical Engineering
Beijing University of Technology
Beijing 100124, PR China
e-mail:hxdai@bjut.edu.cn

***Abstract*—Three-dimensionally ordered macroporous (3DOM) Fe_2O_3 and 0.48–1.95 wt% Au/3DOM Fe_2O_3 catalysts were prepared using the poly(methyl methacrylate)-templating and polyvinyl alcohol-protected reduction methods, respectively. It is found that the porous catalysts with a surface area of 45–46 m^2/g were of a rhombohedral α-Fe_2O_3 crystal structure, and Au nanoparticles (NPs) with a size of 4–6 nm were well dispersed on the3DOM Fe_2O_3 surface. The 1.95Au/3DOM Fe_2O_3 sample possessed the best low-temperature reducibility and showed the highest catalytic activity ($T_{50\%}$ = 162 °C and $T_{90\%}$ = 204 °C at SV = 20,000 mL/(g h)) for toluene oxidation, which was associated with its well-dispersed and small sized Au NPs, good low-temperature reducibility, and strong interaction between Au NPs and 3DOM Fe_2O_3.**

Keywords-three-dimensionally ordered macropore; iron oxide; supported gold catalyst; toluene oxidation; volatile organic compound

I. INTRODUCTION

Most of volatile organic compounds (VOCs) are harmful to the atmosphere and human health. Catalytic oxidation is believed to be an effective pathway for the removal of VOCs, in which the catalyst plays a key role in determining the efficiency of such a process.

In the past years, oxidation of VOCs over transition metal oxide (e.g., Co_3O_4, Mn_3O_4, and Fe_2O_3)-supported precious metal catalysts has been studied. These materials are catalytically active for the oxidation of VOCs. For example, Wang et al. reported that the good catalytic performance for *o*-xylene oxidation of Pd/porous Co_3O_4 was associated with the Pd particle size, oxidized Pd species, and oxygen vacancies in Co_3O_4 [1]. Solsona et al. observed that the Au-deposited partially ordered mesoporous Co_3O_4 catalysts were highly active for toluene oxidation [2]. Ji and coworkers found a strong morphological effect of Mn_3O_4 nanocrystallites on catalytic performance of Au/Mn_3O_4 for benzene combustion [3].

Fe_2O_3 is an important catalytic material due to its low cost, non-toxicity, and high resistance to corrosion [4]. Although iron oxide is less active than cobalt or manganese oxide, it presents a high sintering temperature that can avoid deactivation. It was reported that the iron oxide catalysts showed moderate activity for the total oxidation of lower alkanes (e.g., propane and propene) at low temperatures [5]. The Fe_2O_3-supported noble metal catalysts were more active than those supported on other materials [6]. Gold nanoparticles (NPs) supported on reducible transition-metal oxides (e.g., Fe_2O_3) show good catalytic activities for VOCs oxidation. Simona et al. [7,8] examined the activities of the Au/Fe_2O_3 catalysts for the oxidation of numerous VOCs (methanol, methanol, propanol, acetone, and toluene), and found that the highly dispersed Au NPs could activate the gas-phase oxygen molecules and undermine the strength of Fe–O bonds, thus improving the performance of the Fe_2O_3-supported Au samples.

Using the poly (methyl methacrylate) (PMMA) as hard template and methanol-ethyl glycol as solvent, Masahiroet al. [9] prepared the three-dimensionally ordered macroporous (3DOM) Fe_2O_3 samples with a surface area of 13–57 m^2/g. Previously, we used the PMMA-templating strategy to generate 3DOM Fe_2O_3 materials with a surface area of 32–46 m^2/g [10]. However, there have been no reports on the use of three-dimensionally ordered macroporous (3DOM) Fe_2O_3-supported gold catalysts for the oxidation of toluene. In this work, we report the fabrication of the Au/3DOM Fe_2O_3 catalysts using the PMMA-templating and polyvinyl alcohol (PVA)-protected reduction methods and their catalytic performance for the oxidation of toluene.

II. EXPERIMENTAL

A. Catalyst Preparation

Well-packed monodispersive colloidal crystal template, PMMA microspheres with an average diameter of ca. 300 nm, was synthesized using the approach reported elsewhere [11]. The macroporous Fe_2O_3 samples with crystalline mesoporous walls were fabricated using the dual templating strategy. In a typical synthesis, 10 mmol of Fe $(NO_3)_3 \cdot 9H_2O$ and 1.0 g of P123 ($M_{av.}$ = 5800 g/mol) were dissolved in 10 mL of absolute EtOH or in 10 mL of anhydrous EG and MeOH mixed solution (EG/MeOH volumetric ratio = 3/2) under ultrasonic radiation (90 Hz), in which iron nitrate concentration of the resulting solution was 1 mol/L and the molar ratio of Fe/P123 was 232. 3.0 g of highly ordered PMMA microspheres was added and soaked by the above mixed solution. After the PMMA microspheres were thoroughly wetted, the excessive liquid was filtered via a Buchner funnel connected to vacuum (0.07 MPa). The obtained intermediate was dried in a desiccator using

anhydrous calcium chloride as desiccating agent (relative humidity < 50 %) at room temperature (RT) for 12 h, and calcined in air at a ramp of 1°C/min from RT to 300°C and kept at this temperature for 3 h, and then to 550°C at the same heating rate and maintained at this temperature for 3 h, thus obtaining the porous iron oxide products.

The 3DOM Fe_2O_3-supported gold NPs with different Au loadings (*x*Au/3DOM Fe_2O_3, theoretical gold loading x = 0.5, 1.0, and 2.0 wt%) were prepared using a polyvinyl alcohol (PVA)-protected reduction method. The typical preparation procedures are as follows: (i) The noble metal aqueous solution (0.01 mol/L) was in advance prepared with $HAuCl_4$ as noble metal source; (ii) a stoichiometric amount of the noble metal aqueous solution was first diluted with deionized water to be 1/50 of the original concentration, and a desired amount of PVA was then added to the above aqueous solution (Au/PVA mass ratio = 1.0: 1.5) in an ice–water bath under vigorous stirring for 10 min; (iii) after rapidly injecting the 0.1 mol/L $NaBH_4$ aqueous solution (Au/$NaBH_4$ molar ratio = 1.0 : 5.0) and continuously stirring for 20 min, a sol was obtained; (iv) a desired amount of the 3DOM Fe_2O_3 support was added to the sol, and the obtained suspension was subjected to sonication (60 kHz) for 30 s. A N_2 bubble-assisted stirring operation was adopted to agitate the suspension for 10 h until complete adsorption of colloidal noble metals occurred; and (v) the solid was filtered, washed with 2.0 L of deionized water, dried at 80°C for 12 h, and calcined in air at a ramp of 1°C/min from RT to 550°C and maintained at this temperature for 3 h, thus obtaining the *x*Au/3DOM Fe_2O_3 samples. The results of inductively coupled plasma atomic emission spectroscopic (ICP–AES, Thermo Electron IRIS Intrepid ER/S) studies show that the real Au loadings (x) in *x*Au/3DOM Fe_2O_3 were 0.48, 0.97, and 1.95 wt%, respectively.

For comparison purposes, we also prepared a nonporous iron oxide sample (denoted as Fe_2O_3–Bulk) by calcining a certain amount of ferric nitrate in air at 650°C for 3 h and the 1.98Au/Fe_2O_3–Bulk sample by using the polyvinyl alcohol (PVA)-protected reduction method after calcination at 550°C for 3 h.

All of the chemicals (A.R. in purity) were purchased from Beijing Sinopharm Chemical Reagents Company and used without further purification.

B. Catalyst Characterization

The real Au contents in the samples were measured using the inductively coupled plasma atomic emission spectroscopic (ICP–AES) technique on a Thermo Electron IRIS Intrepid ER/S spectrometer. The samples were dissolved in a mixture of concentrated HCl and HNO_3 with volumetric ratio of 3/1 prior to the analysis. X-ray diffraction (XRD) patterns of the samples were recorded on a Bruker D8 Advance diffractometer with Cu Kα radiation and nickel filter (λ = 0.15406 nm). The Brunauer-Emmett-Teller surface areas of the samples were calculated on the basis of the N_2 adsorption-desorption isotherms obtained on a Micromeritics ASAP 2020 analyzer. The scanning electron microscopic (SEM) and transmission electron microscopic (TEM) images of the samples were recorded on a Gemini Zeiss Supra 55 apparatus (operating at 10 kV) and a JEOL-2010 equipment (operating at 200 kV), respectively. Thermogravimetric analysis (TGA) and differential scanning calorimetric (DSC) analysis were conducted on a SDT Q600 (TA) apparatus in an air flow of 100 mL/min from room temperature to 700°C (heating rate: 10°C/min).

Hydrogen temperature-programmed reduction (H_2-TPR) experiments were carried out on a chemical adsorption analyzer (Autochem II 2920, Micromeritics). Before TPR measurement, ca. 0.02 g of catalyst (40−60 mesh) was loaded to a quartz fixed-bed U-shaped microreactor (i.d. = 4 mm) and pretreated in an O_2 flow of 30 mL/min at 300°C for 1 h. After being cooled at the same atmosphere to RT, the pretreated sample was exposed to a flow (50 mL/min) of 5 % H_2−95 % Ar (*v*/*v*) mixture and heated from RT to 600°C at a ramp of 10°C/min. The alteration in H_2 concentration of the effluent was monitored online by the chemical adsorption analyzer, and the H_2-TPR profiles of the samples were obtained.

C. Catalytic Activity Evaluation

Catalytic activities of the samples for the oxidation of toluene were tested in a continuous flow fixed-bed quartz microreactor (i.d. = 4 mm). In order to minimize the effect of hot spots, 0.25 g of quartz sands (40–60 mesh) was mixed with 50 mg of the catalyst (40–60 mesh). The catalyst was pretreated in 30 mL/min O_2 flow at 250°C for 1 h before the test. After being cooled to RT, the reactant mixture (1000 ppm toluene + O_2 + N_2 (balance)) with a flow rate of 16.7 mL/min was passed through the catalyst bed. The toluene/O_2 molar ratio was 1/400 and the space velocity (SV) was ca. 20,000 mL/(g h). We changed the catalyst mass for the alteration of SV. The reactants and products were analyzed online on a gas chromatograph (GC-2010, Shimadzu), equipped with a stabilwax@-DA column (30 m in length) for organic separation and a Carboxen 1000 column (3 m in length) for permanent gas separation.

III. RESULTS AND DISCUSSION

A. Crystal Structure, Morphology, and Surface Area

Figure 1 shows the XRD patterns of the samples. It is observed that the crystal structure of the as-obtained samples could be indexed to the rhombohedral α-Fe_2O_3 phase (JCPDS PDF# 86-2368), as indicated in figure 1e. Similar results have been reported by other researchers [12, 13]. The loading of Au did not change the crystal structure of Fe_2O_3. The detection of a weak diffraction peak at 2θ = 38.5° due to the Au (111) plane (JCPDS PDF# 04-0784) indicates the generation of cubic Au NPs in the 0.97Au/3DOM Fe_2O_3, 1.95Au/3DOM Fe_2O_3, and 1.98Au/Fe_2O_3-Bulk samples (Figure 1c–e). The difference in peak intensity suggests that the 3DOM-structured samples possessed a lower crystallinity than the bulk Fe_2O_3 supported Au sample.

Figure 2 shows the representative SEM images of the porous samples. It can be seen that the Fe_2O_3 and its supported Au samples displayed a high-quality 3DOM architecture, with the typical marcopore sizes being 140–180

nm. The loading of Au NPs did not induce a significant alteration in particle morphology. Figure 3 shows the TEM images of the porous samples. It is observed that the Au NPs

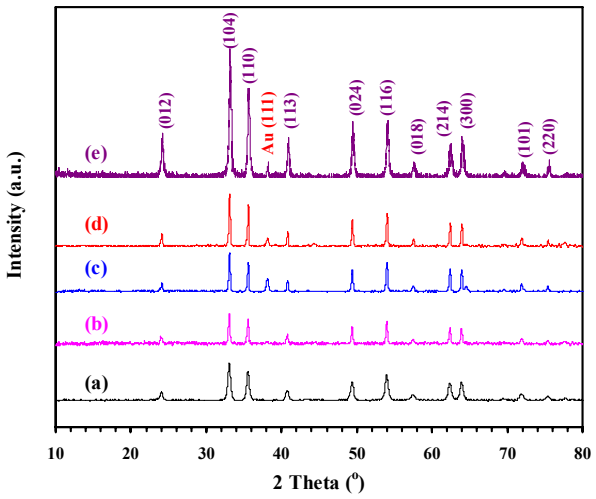

Figure 1. XRD patterns of (a) 3DOM Fe_2O_3, (b) 0.48Au/3DOM Fe_2O_3, (c) 0.97Au/3DOM Fe_2O_3, (d) 1.95Au/3DOM Fe_2O_3, and (e) 1.98Au/Fe_2O_3-Bulk.

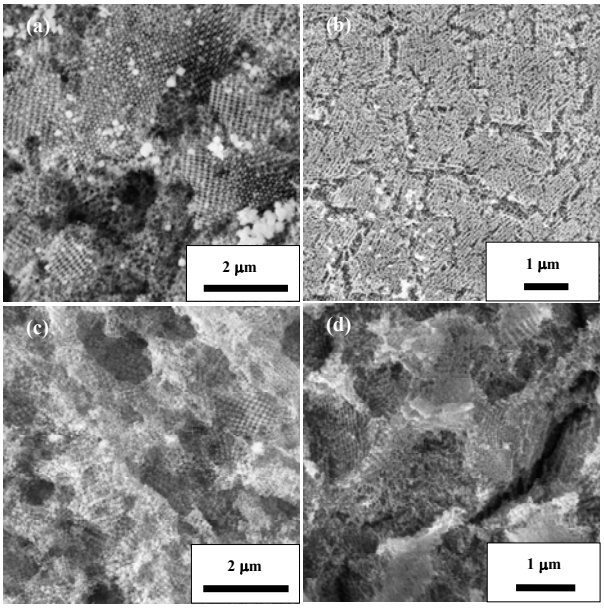

Figure 2. SEM images of (a) 3DOM Fe_2O_3, (b) 0.48Au/3DOM Fe_2O_3, (c) 0.97Au/3DOM Fe_2O_3, and (d) 1.95Au/3DOM Fe_2O_3.

were well dispersed on the surface of 3DOM Fe_2O_3. The average Au NP diameter of each sample was calculated by making a statistic analysis on the sizes of more than 200 Au NPs in the TEM images. The average Au particle sizes of the 0.48Au/3DOM Fe_2O_3, 0.97Au/3DOM Fe_2O_3, 1.95Au/3DOM Fe_2O_3, and 1.98Au/Fe_2O_3-Bulk samples were 6, 5, 4, and 12 nm, respectively. Surface areas of the 3DOM Fe_2O_3 and *x*Au/3DOM Fe_2O_3 (*x* = 0.48, 0.97, and 1.95 wt %) samples were 46.2, 45.1, 45.3, and 44.9 m^2/g, respectively, whereas that of the 1.98Au/Fe_2O_3-Bulk sample was 7.6 m^2/g.

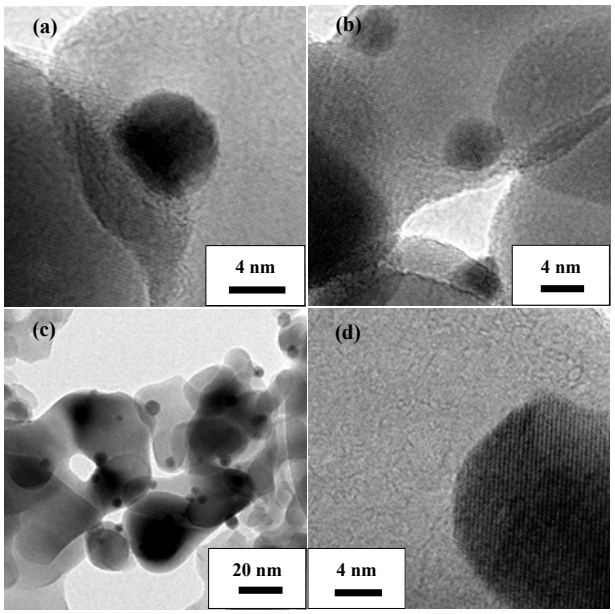

Figure 3. TEM images of (a) 0.48Au/3DOM Fe_2O_3, (b) 0.97Au/3DOM Fe_2O_3, (c) 1.95Au/3DOM Fe_2O_3, and (d) 1.98Au/Fe_2O_3-Bulk.

B. *Thermal Stability*

To examine the thermal stability, we carried out the TGA/DTA experiment of the 3DOM Fe_2O_3 precursor. Figure 4 illustrates the TGA/DTA profiles of the 3DOM Fe_2O_3 sample before calcination. It is observed that there were weight losses of ca. 8.9 and 88.8 wt% in the temperature range of 30–160 and 160–375°C, accompanying by the appearance of well-resolved endothermic signals centered at 134 and 366°C, respectively. The two weight losses could be attributed to the removal of adsorbed water or organics (EtOH, EG, and MeOH) and the decomposition of $Fe(NO_3)_3$ [14] as well as the oxidation of PMMA [9,11]. The result clearly demonstrates that calcining the sample intermediate above 550°C was appropriate to generate the Fe_2O_3 crystals.

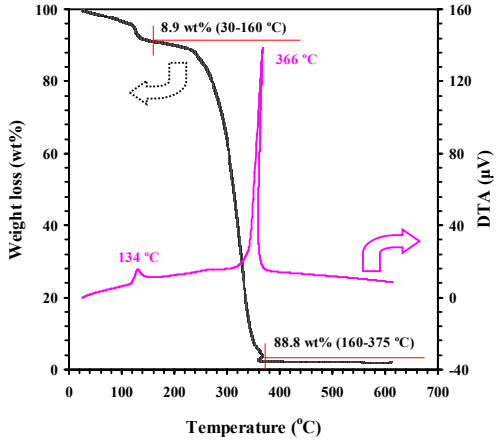

Figure 4. TGA/DTA profiles of the 3DOM Fe_2O_3 sample before calcination.

C. *Reducibility*

Reducibility of a transition metal oxide is highly related to its catalytic performance. Usually, the reduction of iron oxide proceeds via the order of $Fe_2O_3 \rightarrow Fe_3O_4 \rightarrow Fe^0$ [15, 16]. Figure 5 illustrates the H_2-TPR profiles of the as-fabricated samples. For each sample, two reduction steps were clearly observed in the range of 30–300 and 300–600°C. The first step was due to the removal of adsorbed oxygen species and the reduction of oxidized gold ($Au^{\delta+}$) species and Fe_2O_3 to Au^0 and Fe_3O_4 [17,18], respectively, whereas the second step was due to the reduction of Fe_3O_4 to Fe^0 [15,17,18]. With the rise in Au loading from 0.48 to 1.95-wt%, the reduction peaks shifted to lower temperatures (especially temperature of the first reduction peak decreased

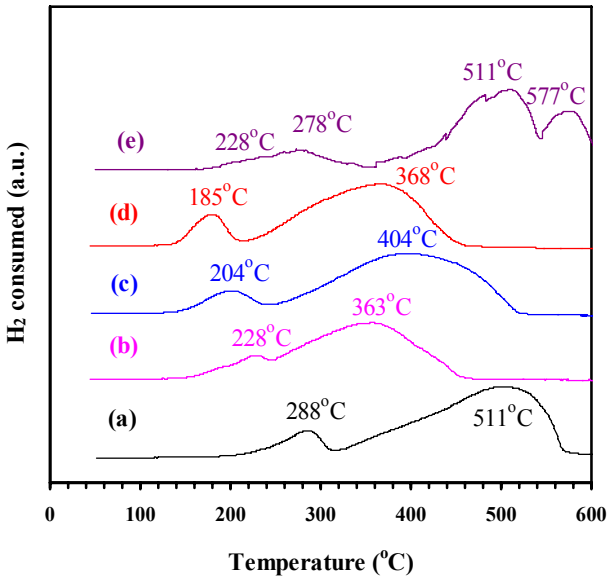

Figure 5. H_2-TPR profiles of (a) 3DOM Fe_2O_3, (b) 0.48Au/3DOM Fe_2O_3, (c) 0.97Au/3DOM Fe_2O_3, (d) 1.95Au/3DOM Fe_2O_3, and (e) 1.98Au/Fe_2O_3-Bulk.

to 185°C for the 1.95Au/3DOM Fe_2O_3 sample), indicating that the loading of Au NPs improved the low-temperature reducibility. On the other hand, the shit in reduction temperature also suggests the presence of a strong interaction between Au NPs and 3DOM Fe_2O_3. The 1.98Au/Fe_2O_3-Bulk sample showed four reduction peaks at 228, 278, 511, and 577°C: the former two were the removal of adsorbed oxygen species and the reduction of $Au^{\delta+}$ to Au^0 and Fe_2O_3 to Fe_3O_4 [17, 18], while the latter two were the reduction of Fe_3O_4 to Fe^0 [15,17,18]. From the H_2-TPR results, one can realize that the 1.95Au/3DOM Fe_2O_3 sample exhibited the best low-temperature reducibility. The low-temperature reducibility increased in the order of 3DOM Fe_2O_3 < 0.48Au/3DOM Fe_2O_3 < 1.98Au/Fe_2O_3-Bulk < 0.97Au/3DOM Fe_2O_3 < 1.95Au/3DOM Fe_2O_3.

D. *Catalytic Performance*

Under the conditions of toluene concentration = 1000 ppm, toluene/O_2 molar ratio = 1/400, SV = 20,000 mL/(g h), and temperature < 400°C, no significant conversion of toluene was detected over the quartz sands loaded in the microreactor. That is to say, the complete oxidation of toluene over the present catalysts was a catalytic process. Figure 6 shows the catalytic activities of the samples for toluene oxidation. It is observed that toluene conversion increased

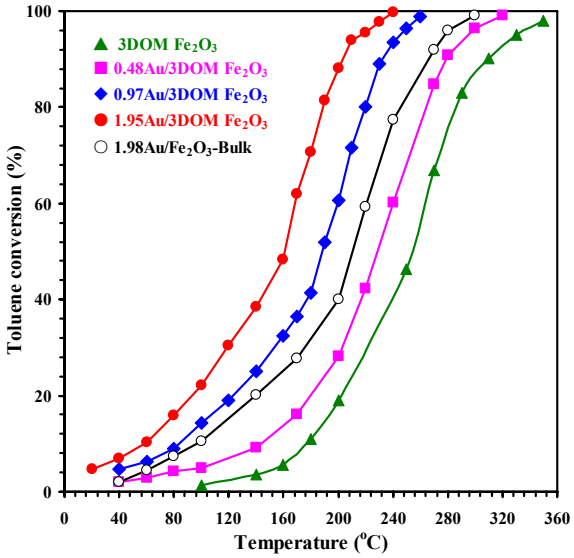

Figure 6. Toluene conversion versus reaction temperature over the as-prepared samples under the conditions of toluene concentration = 1000 ppm, toluene/O_2 molar ratio = 1/400, and SV = 20,000 mL/(g h).

TABLE I. CATALYTIC ACTIVITIES OVER THE AS-PREPARED SAMPLES UNDER THE CONDITIONS OF TOLUENE CONCENTRATION = 1000 ppm, TOLUENE/O_2 MOLAR RATIO = 1/400, AND SV = 20,000 mL/(g h).

Sample	Toluene oxidation activity (°C)		
	$T_{10\%}$	$T_{50\%}$	$T_{90\%}$
3DOM Fe_2O_3	180	256	311
0.48Au/3DOM Fe_2O_3	146	230	280
0.97Au/3DOM Fe_2O_3	88	190	236
1.95Au/3DOM Fe_2O_3	60	162	204
1.98Au/Fe_2O_3-Bulk	100	212	268

with a rise in temperature. For better comparison purposes, the reaction temperatures $T_{10\%}$, $T_{50\%}$, and $T_{90\%}$ (corresponding to toluene conversion = 10, 50, and 90 %) were summarized in Table I. the $T_{10\%}$, $T_{50\%}$, and $T_{90\%}$ were 180, 256, and 311°C over the 3DOM Fe_2O_3 sample, respectively. Previously, Fe_2O_3 was employed as catalyst for the removal of toluene. For example, Scirè and coworkers observed a $T_{90\%}$ of 380°C over Fe_2O_3 for toluene oxidation at SV = 186 mL/(g h) [8]. Duran et al. reported that 80 % toluene conversion could be achieved over Fe_2O_3 at 365°C and 20,000 mL/(g h) [19]. Therefore, our 3DOM Fe_2O_3 sample outperformed the Fe_2O_3 samples reported above [8, 19]. With the loading of Au NPs, the catalytic activity was much improved. Over the

1.98Au/Fe_2O_3-Bulk sample, the $T_{10\%}$, $T_{50\%}$, and $T_{90\%}$ were 100, 212, and 268°C, respectively. Obviously, the 1.95Au/3DOM Fe_2O_3 sample performed the best: $T_{10\%}$ = 60°C, $T_{50\%}$ = 162°C, and $T_{90\%}$ = 204°C. Therefore, the catalytic activity increased in the order of 3DOM Fe_2O_3 < 0.48Au/3DOM Fe_2O_3 < 1.98Au/Fe_2O_3-Bulk < 0.97Au/3DOM Fe_2O_3 < 1.95Au/3DOM Fe_2O_3, coinciding with the sequence in low-temperature reducibility of these samples (Figure 5). The catalytic activity of the 1.95Au/3DOM Fe_2O_3 sample was much better than that sample ($T_{50\%}$ = 200°C and $T_{90\%}$ = 260°C at SV = 20,000 mL/(g h)) of the 6.55Au/Fe_2O_3 nanodisk sample reported in the literature [20].

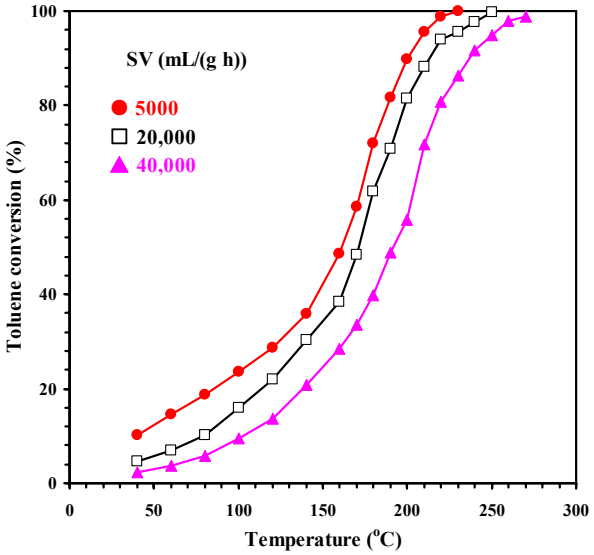

Figure 7. Effect of SV on the catalytic activity over the 1.95Au/3DOM Fe_2O_3 sample.

Due to the presence of strong interaction between Au NPs and Fe_2O_3, partial Au^0 might react with Fe^{3+} to generate $Au^{\delta+}$ and Fe^{2+} species, causing the surface Fe^{2+} and $Au^{\delta+}$ concentrations to increase. According to the electroneutrality principle, an increase in Fe^{2+} content can give a rise in amount of oxygen vacancies (Table I). The generation of surface oxygen vacancies facilitates the activation of gas-phase oxygen molecules and the easy replenishment of adsorbed oxygen (O_{ads}) species. The oxidation of organic compounds usually proceeds through the interaction of organic compounds with O_{ads} species at oxygen vacancies. During the oxidation process of toluene over xAu/Fe_2O_3, the reduction of transition metal ions was associated with the reducibility of the samples, and the generation of oxygen vacancies took place concurrently. That is to say, an enhancement in reducibility would be beneficial for the generation of oxygen vacancies, and then for the activation of gas-phase oxygen molecules and the replenishment of O_{ads} species. Therefore, it is understandable that the better low-temperature reducibility led to better catalytic performance in the present study. There are several kinds of active sites (noble metal, transition metal oxide, and interfaces between noble metal and transition metal oxide) in the reducible metal oxide-supported noble metal catalysts. As we know, the Au particle size is an important factor influencing catalytic activity of a supported Au sample [21]. In the present study, the average size of Au NPs in 1.95Au/3DOM Fe_2O_3 was 4 nm, whereas that in 1.98Au/Fe_2O_3-Bulk was 12 nm. Therefore, it is understandable that the 1.95Au/3DOM Fe_2O_3 sample performed better than 1.98Au/Fe_2O_3-Bulk for toluene oxidation. Figure 7 shows the effect of SV on catalytic activity of the 1.95Au/3DOM Fe_2O_3 sample. It is observed that toluene conversion increased with the drop in SV, which might be a result due to the elongation of contact time between reactant molecules and catalyst.

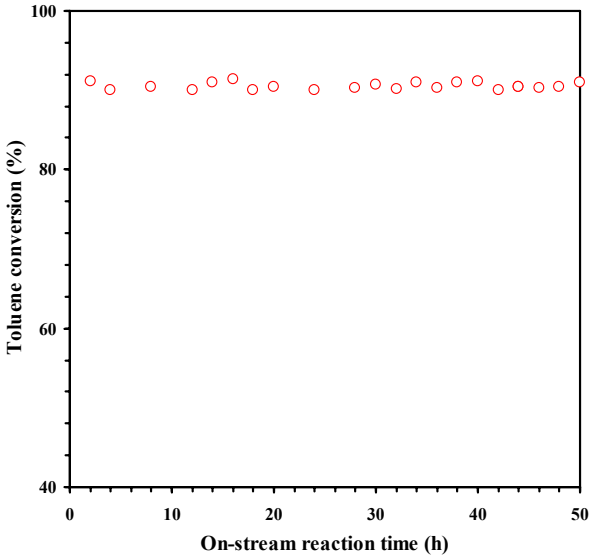

Figure 8. Toluene conversion as a function of on-stream reaction time over the 1.95Au/3DOM Fe_2O_3 sample at 204°C and SV = 20,000 mL/(g h).

In order to evaluate the catalytic stability, 50-h on-stream toluene oxidation experiment at 204°C over the 1.95Au/3DOM Fe_2O_3 sample was carried out. Under the adopted reaction conditions, no significant loss in catalytic activity was detected within 50 h of on-stream reaction (Figure 8), demonstrating the 1.95Au/3DOM Fe_2O_3 sample was catalytically durable.

IV. CONCLUSIONS

3DOM Fe_2O_3 and 0.48–1.95Au/3DOM Fe_2O_3 catalysts were prepared using the PMMA-templating and PVA-protected reduction methods, respectively. The 3DOM Fe_2O_3 and 0.48–1.95Au/3DOM Fe_2O_3 catalysts possessed a rhombohedral α-Fe_2O_3 crystal structure and a surface area of 45–46 m^2/g. Au NPs with a size of 4–6 nm were highly dispersed on the surface of 3DOM Fe_2O_3. Catalytic activity for toluene oxidation enhanced with the loading of Au NPs, with the 1.95Au/3DOM Fe_2O_3 sample showing the highest catalytic activity ($T_{50\%}$ = 162°C and $T_{90\%}$ = 204°C at SV = 20,000 mL/(g h)). It is concluded that the good catalytic performance of 1.95Au/3DOM Fe_2O_3 was associated with its

highly dispersed Au NPs and better low-temperature reducibility as well as the strong interaction between Au NPs and 3DOM Fe_2O_3.

ACKNOWLEDGMENT

The work described was supported by the NSF of China (21377008), National High Technology Research and Development Program ("863" Program) of China (2015AA034603), Foundation on the Creative Research Team Construction Promotion Project of Beijing Municipal Institutions, and Scientific Research Base Construction–Science and Technology Creation Platform National Materials Research Base Construction.

REFERENCES

[1] Y. F. Wang, C. B. Zhang, F. D. Liu, and H. He, "Well-Dispersed Palladium Supported on Ordered Mesoporous Co_3O_4 for Catalytic Oxidation of *o*-Xylene," Appl. Catal. B, vol. 142–143, Oct.-Nov. 2013, pp. 72-79, doi: 10.1016/j.apcatb.2013.05.003.

[2] B. Solsona, E. Aylón, R. Murillo, A. M. Mastral, A. Monzonís, S. Agouram, T. E. Davies, S. H. Taylor, and T. Garcia, "Deep Oxidation of Pollutants Using Gold Deposited on a High Surface Area Cobalt Oxide Pprepared by a Nanocasting Route," J. Hazard. Mater, vol. 187, Mar. 2011, pp. 544-552, doi:10.1016/j.jhazmat.2011.01.073.

[3] Z.Y. Fei, B. Sun, L. Zhao, W.J. Ji, and C.-T. Au, "Strong Morphological Effect of Mn_3O_4 Nanocrystallites on the Catalytic Activity of Mn_3O_4 and Au/Mn_3O_4 in Benzene Combustion," Chem. Eur. J., vol. 19, May 2013, pp. 6480-6487, doi:10.1002/chem.201204112.

[4] J. B. Lian, X. C. Duan, J. Ma, P. Peng, T. Kim, and W. J. Zheng, "Hematite (α-Fe_2O_3) with Various Morphologies: Ionic Liquid-Assisted Synthesis, Formation Mechanism, and Properties," ACS Nano, vol. 3, Nov. 2009, pp. 3749-3761, doi: 10.1021/nn900941e.

[5] M. Baldi, V. Sánchez-Escribano, J. M. G Amores, F. Milella, and G. Busca, "Characterization of Manganese and Iron Oxides as Combustion Catalysts for Propane and Propene," Appl. Catal. B, vol. 17, Jul. 1998, pp. L175–L182, doi:10.1016/S0926-3373(98)00013-7.

[6] M. C. Kung, R. J. Davis, and H. H. Kung, "Understanding Au-Catalyzed Low-Temperature CO Oxidation," J. Phys. Chem. C, vol. 111, Aug. 2007, pp. 11767-11775, doi: 10.1021/jp072102i.

[7] S. Minicò, S. Scirè, C. Crisafulli, R. Maggiore, and S. Galvagno, "Catalytic Combustion of Volatile Organic Compounds on Gold/Iron Oxide Catalysts," Appl. Catal. B, vol. 28, Dec. 2000, pp. 245-251, doi: 10.1016/S0926-3373 (00) 00181-8.

[8] S. Minicò, S. Scirè, C. Crisafulli, and S. Galvagno, "Influence of Catalyst Pretreatments on Volatile Organic Compounds Oxidation over Gold/Iron Oxide," Appl. Catal. B, vol. 34, Nov. 2001, pp. 277-285, doi: 10.1016/S0926-3373(01)00221-1.

[9] M. Sadakane, T. Horiuchi, N. Kato, C. Takahashi, and W. Ueda, "Facile Preparation of Three-Dimensionally Ordered Macroporous Alumina, Iron Oxide, Chromium Oxide, Manganese Oxide, and Their Mixed-Metal Oxides with High Porosity," Chem. Mater., vol. 19, Nov. 2007, 5779-5785, doi:10.1021/cm071823r.

[10] R. Z. Zhang, H. X.Dai, Y. C. Du, L. Zhang, J. G. Deng, Y. S. Xia, Z. X. Zhao, X. Meng, and Y. X. Liu, "P123-PMMA Dual-Templating Generation and Unique Physicochemical Properties of Three-Dimensionally Ordered Macroporous Iron Oxides with Nanovoids in the Crystalline Walls," Inorg. Chem., vol. 50, Mar. 2011, pp. 2534-2544, doi: 10.1021/ic1023604.

[11] H. N. Li, L. Zhang, H. X. Dai, and H. He, "Facile Synthesis and Unique Physicochemical Properties of Three-Dimensionally Ordered Macroporous Magnesium Oxide, Gamma-Alumina, and Ceria-Zirconia Solid Solutions with Crystalline Mesoporous Walls," Inorg. Chem., vol. 48, May 2009, pp. 4421-4434, doi: 10.1021/ic900132k.

[12] T. P. Raming, A. J. A. Winnubst, C. M. Kats, and A. P. Philipse, "The Synthesis and Magnetic Properties of Nanosized Hematite (α-Fe_2O_3) Particles," J. Colloid Interface Sci., vol. 249, May 2002, pp. 346-350, doi: 10.1006/jcis.2001.8194.

[13] P. P. Sarangi, B. Naik, and N. N. Ghosh, "Low Temperature Synthesis of Single-Phase Alpha-Fe_2O_3 Nano-Powders by Using Simple but Novel Chemical Methods," Powder Technol., vol. 192, Jun. 2002, pp. 245-249, doi: 10.1016/j.powtec.2009.01.002.

[14] Z. Gabelica, A. Charmot, R. Vataj, R. Soulimane, J. Barrault, and S. Valange, "Thermal Degradation of Iron Chelate Complexes Adsorbed on Mesoporous Silica and Alumina," J. Therm. Anal. Cal., vol. 95, Feb. 2009, pp. 445-454, doi: 10.1007/s10973-008-9256-z.

[15] C. S. Castro, L. C. A. Olievira, and M. C. Guerreiro, "Effect of Hydrogen Treatment on the Catalytic Activity of Iron Oxide Based Materials Dispersed Over Activated Carbon: Investigations Toward Hydrogen Peroxide Decomposition," Catal. Lett., vol. 133, Nov. 2009, pp. 41-48, doi:10.1007/s10562-009-0167-9.

[16] E. E. Unmuth, L. H. Schwarta, and J. B. Butt, "Iron Alloy Fischer-Tropsch Catalysts: I. Oxidation-Reduction Studies of the Fe-Ni System," J. Catal., vol. 61, Jan. 1980, pp. 242-255, doi:10.1016/0021-9517(80)90360-7.

[17] E. Rombi, I. Ferino, R. Monaci, C. Picciau, V. Solinas, and R. Buzzoni, "Toluene Ammoxidation on α-Fe_2O_3-Based Catalysts," Appl. Catal. A, vol. 266, Jul. 2004, pp. 73-79. doi:10.1016/j.apcata.2004.01.028.

[18] Q. J. Yang, H. Choi, S. R. Al-Abed, and D. D. Dionysiou, "Iron–Cobalt Mixed Oxide Nanocatalysts: Heterogeneous Peroxymonosulfate Activation, Cobalt Leaching, and Ferromagnetic Properties for Environmental Applications," Appl. Catal. B, vol. 88, May 2009, pp. 462-469, doi: 10.1016/j.apcatb.2008.10.013.

[19] F. G. Durán, B. P. Barbero, L. E. Cadús, C. Rojas, M. A. Centeno, and J. A. Odriozola, "Manganese and Iron Oxides as Combustion Catalysts of Volatile Organic Compounds," Appl. Catal. B, vol. 92, Oct. 2009, pp. 194-201, doi: 10.1016/j.jcat.2003.12.014.

[20] W. Han, J.G. Deng, S. H. Xie, H. G. Yang, H. X. Dai, and C. T. Au, "Gold Supported on Iron Oxide Nanodisk as Efficient Catalyst for the Removal of Toluene," Ind. Eng. Chem. Res., vol. 53, Mar. 2014, pp. 3486-3494. doi: 10.1021/ie5000505.

[21] M. Valden, X. Lai, and D. W. Goodman, "Onset of Catalytic Activity of Gold Clusters on Titania with the Appearance of Nonmetallic Properties," Science, vol. 281, Sept. 1998, pp. 1647-1650, doi: 10.1126/science.281.5383.1647.